Journal of Power Sources 244 (2013) 538–543

Contents lists available at SciVerse ScienceDirect

Journal of Power Sources

journal homepage: www.elsevier.com/locate/jpowsour

Short communication

Monodispersed hollow carbon/Fe_3O_4 composite microspheres for high performance anode materials in lithium-ion batteries

Jun-Ki Hwang [a], Hyung-Seok Lim [a], Yang-Kook Sun [b,**], Kyung-Do Suh [a,*]

[a] Department of Chemical Engineering, College of Engineering, Hanyang University, Seoul 133-791, Republic of Korea
[b] Department of WCU Energy Engineering, College of Engineering, Hanyang University, Seoul 133-791, Republic of Korea

HIGHLIGHTS

- Monodispersed hollow carbon/Fe_3O_4 microspheres exhibit excellent rate performance.
- Formation of Fe_3O_4 nano-crystals affects the shell thickness and surface morphologies.
- High reversible capacities can be remained at various current rates from 0.1 to 10C.
- The excellent cycling and rate performance can be attributed to the hollow structure.

ARTICLE INFO

Article history:
Received 7 November 2012
Received in revised form
4 February 2013
Accepted 8 February 2013
Available online 16 February 2013

Keywords:
Hollow structure
Carbon
Magnetite
Carbon/magnetite composite
Anode materials
Lithium ion battery

ABSTRACT

Monodispersed carbon/Fe_3O_4 composite microspheres with hollow structures are prepared by heat treating monodispersed hollow poly(St/AN/DVB)/Fe_3O_4 microspheres synthesized through seeded polymerization and a wet chemical method. Monodispersed hollow carbon/Fe_3O_4 composite microspheres are characterized by optical microscopy, scanning electron microscopy, focused-ion beam scanning electron microscopy and transmission electron microscopy, X-ray diffraction. The electrodes containing the monodispersed hollow carbon/Fe_3O_4 composite microspheres exhibit an excellent cycling and rate capabilities with efficiency of 99% even after 100 cycles at high current rate. These results are because hollow structure and Fe_3O_4 nano-crystals introduced significantly affected the kinetics of lithium ions and improvement of low capacity of carbon used as LIBs anodes.

1. Introduction

Lithium ion batteries (LIBs) have been widely used as power sources for various portable electronic devices, including cellular phones, lap top computers, and tablet PCs. They are also expected to be important power sources for future applications in electric vehicles and energy storage systems [1]. High specific energy density, cycle stability, and low cost are qualities and characteristics needed for future applications of LIBs. To improve cell performance, many research groups have suggested various alternative anode materials such as silicon, intermetallic alloys, and transition metal oxides [2]. Among these materials, magnetite (Fe_3O_4) has been attracting attention as an anode material because of its eco-friendliness, safety, and high specific capacity (926 mAh g^{-1}) [3,4]. However, the Fe_3O_4 electrode shows poor cycling performance due to large volume variation during cycling that causes loss of electrical contact between the active materials and current collector [5,6]. To solve this problem, researchers have focused on fabricating carbon/Fe_3O_4 composite materials with unique structures, such as porous [7,8], nanowire [9], nano-rod [10,11], flower-like [12], and hollow. Among these, hollow structures are favorable for their lithium ion kinetics during lithiation/de-lithiation. These properties are due to a shorter diffusion length and larger surface area than the solid materials [13]. Recently, some research groups have reported that hollow carbon/Fe_3O_4 microspheres can improve electrochemical properties by their unique structure [14,15]. Although these materials have improved rate capability, they showed poor coulombic efficiency and unstable cycling performances at high current rates.

In this study, monodispersed hollow carbon/Fe_3O_4 composite microspheres (HCFMs) were prepared for use as a high performance anode material in LIBs. To prepare spherical polymer

* Corresponding author. Tel.: +82 2 2220 0526; fax: +82 2 2220 4680.
** Corresponding author. Tel.: +82 2 2220 1749; fax: +82 2 2298 5416.
E-mail addresses: yksun@hanyang.ac.kr (Y.-K. Sun), kdsuh@hanyang.ac.kr (K.-D. Suh).

0378-7753/$ – see front matter © 2013 Elsevier B.V. All rights reserved.
http://dx.doi.org/10.1016/j.jpowsour.2013.02.017

microspheres with highly monodisperse size distribution and hollow structures, seeded polymerization was carried out with the polymerization conditions previously reported by our research group. Hollow structures were formed by phase separation of growing polymer chains and solvent in swollen particles during polymerization. Monodispersed hollow poly(St/AN/DVB)/Fe_3O_4 composite microspheres (HPFMs) were prepared by alkaline co-precipitation of $FeCl_2$ and $FeCl_3$ salts ionized in aqueous solution with as-prepared hollow polymer microspheres. The HCFMs were produced by heat treatment, which retains their intrinsic morphology and structure. The electrochemical performance of HCFMs was compared to that of hollow carbon microspheres (HCMs) and nano-sized Fe_3O_4 particles. HCFMs showed excellent cycling and rate performance because their hollow structures significantly affected the kinetics of lithium ions when used as LIBs anodes. Additionally, the HCFM composite electrode showed reversible capacity of 368 mA h^{-1} after 100 cycles, even at the 10C rate. This value is higher than that of HCM composite electrodes (198 mA h^{-1}) at the same current density. Therefore, we believe that HCFM-based anodes could be an alternative anode material with high rate capability and high reversible capacity.

2. Experimental

2.1. Materials

Styrene (St; Junsei Chemical Co.), acrylonitrile (AN; Junsei Chemical Co.), and divinylbenzene (DVB, mixture of isomers, 55%; Fluka Chemical Co.) were used as purchased. Benzoyl peroxide (BPO; Lancaster) and 2,2′-azoisobutyronitrile (AIBN; Junsei Chemical Co.) were re-crystallized before use to remove an inhibitor from methanol. Poly(vinyl pyrrolidone) (PVP-40T, Mw = 4.0×10^4 g mol^{-1}; Junsei Chemical Co.), poly(vinyl alcohol) (PVA, Mw = 8.8×10^4–9.2×10^4 g mol^{-1}, 87–89% hydrolyzed; Sigma–Aldrich), sodium bis(2-ethylhexyl) sulfosuccinate (aerosol-OT; Wako), ethanol (assay 99.9%; Dae-Jung Chem. Co.), sodium lauryl sulfate (SLS, Wako), toluene (assay 99.5%; Dae-Jung Chem. Co.),iron (III) chloride ($FeCl_3 \cdot 6H_2O$, Shinyo Pure Chemicals Co., Ltd), iron (II) chloride tetrahydrate ($FeCl_2 \cdot 4H_2O$, Waco Pure chemical industries, Ltd.), and ammonium hydroxide (NH_4OH, Dae-Jung Chem. Co.) were purchased and used as received.

2.2. Preparation of monodispersed hollow poly(St/AN/DVB) microspheres (HPMs)

The HPMs were prepared by seeded polymerization. First, LPS seed particles were dispersed by dispersion polymerization [16] in 0.25 wt. % SLS water/EtOH (5/1, g/g) solution (SE solution) using a 250 ml four-neck round bottom flask equipped with a reflux condenser, nitrogen inlet apparatus, and a mechanical stirrer. The LPS seed particles dispersed in SE solution were swollen with finely emulsified 1-chloro-dodecane (CD). Throughout the swelling process, stirring speed and temperature were fixed at 200 rpm and room temperature, respectively. After complete disappearance of CD droplets, the second monomer mixture of AN, DVB, BPO and toluene was emulsified and added to the reactor for another 3 h of swelling. Swollen particles were stabilized with a 5 wt. % PVA aqueous solution and then polymerized at 80 °C for 12 h. The resulting particles were washed repeatedly using water and alcohol, followed by drying at 50 °C.

2.3. Preparation of HCFMs

HPFMs were synthesized by a wet chemical method. HPMs (1 g) were dispersed in water (100 g) with mechanical stirring at 200 rpm. A solution containing 0.470 g $FeCl_2 \cdot 4H_2O$ and 0.172 g $FeCl_3 \cdot 6H_2O$ dissolved in water was placed in the reactor and mixed by mechanical stirring for 24 h. Then, 1.0 ml ammonium hydroxide was added to the reactor and mixed under nitrogen gas at 80 °C for 30 min. The heat treatment was carried out with HPFMs for carbonized HCFMs. The heating process was performed at 600 °C for 7 h in nitrogen gas with a heating rate of 2 °C min^{-1}. To compare their electrochemical properties, HCMs were also prepared by heat treatment at 600 °C for 7 h in nitrogen gas with HPMs.

2.4. Characterization

The particle morphologies were observed using scanning electron microscopy (SEM, JSM-6300, JEOL), optical microscopy (OM, Olympus, BX51), transmission electron microscopy (TEM, JEOL,JEM 2100F),and focused ion beam scanning electron microscopy (FIB-SEM Hitachi, S-4800). The crystallinity of each sample was confirmed using X-ray diffraction patterns. The carbon content of obtained HCFMs was calculated via thermogravimetric analysis (TGA, TG209F3, NETZSCH).

2.5. Electrochemical test

The negative electrode was prepared by coating N-methyl pyrrolidone (NMP)-based slurry containing HCFMs, super-P carbon,

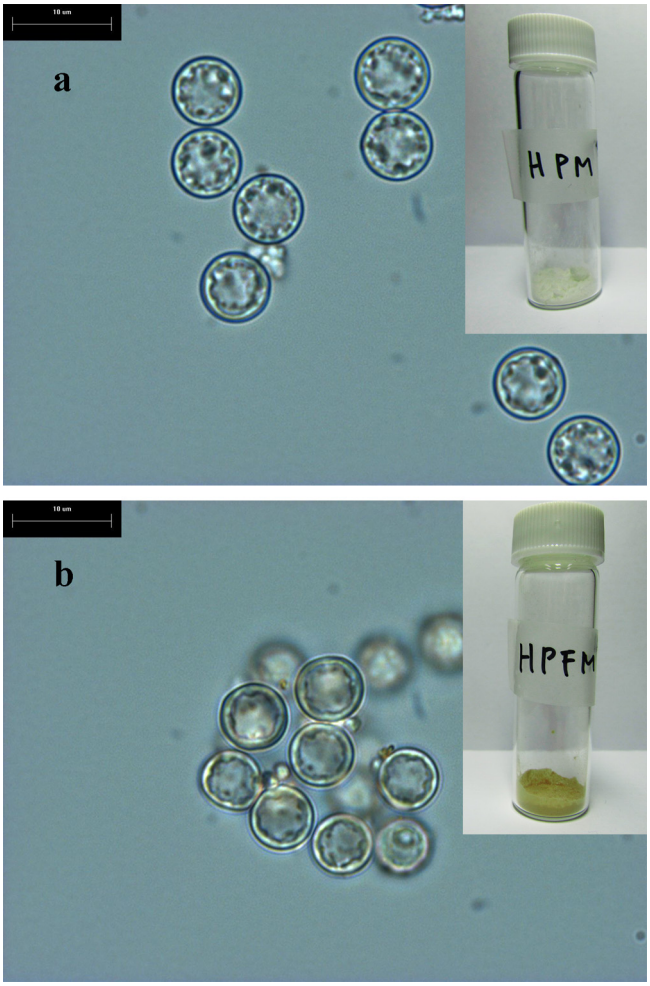

Fig. 1. Optical microscope images of (a) HPMs and (b) brown HPFMs. (For interpretation of the references to color in this figure legend, the reader is referred to the web version of this article.)

and polyvinylidene fluoride (PVdF) (6:3:1) onto copper foil. The electrodes were dried for 20 min at 110 °C and for 4 h at 80 °C in a vacuum until integration into the cell. Li metal foil (1 mm thick) was used as a counter electrode, and a Celgard 2400 microporous polypropylene membrane was used as the separator. The commercial electrolyte consisted of 1 M $LiPF_6$ salt in a mixture of ethylene carbonate (EC)/diethyl carbonate (DEC) (1:1 by volume, provided by Techno Semichem Co., Ltd., Korea). To evaluate the potential applicability of HCFMs in lithium-ion batteries, coin-type cells (2032) with a cutoff voltage of 0.02–3.0 V were used at room temperature (30 °C).

3. Results and discussion

The HCFMs were fabricated by heat-treating synthesized HPFMs via seeded polymerization and co-precipitation of iron salts. First, the HPMs were synthesized by seeded polymerization using linear polystyrene (LPS) as seed particles. The hollow structure of HPMs was constructed by phase separation of toluene and growing polymer chain in swollen LPS particles during polymerization. The Fe_3O_4 nano-crystals were then introduced to the HPMs by co-precipitation of ionized iron salts. Finally, HFPMs were carbonized by heat treatment at high temperature.

3.1. Characteristics of HCFMs

Fig. 1 shows OM images of (a) HPMs and (b) HPFMs and (insets) photographs of the dried powders. In case of HPFMs, after adding ammonium hydroxide, particles became brown, with small brown nanoparticles of similar average diameter, as shown in Fig. 1b. Fig. 1a and b insets show that dried powders have quite different colors.

Fig. 2 shows SEM and FIB-SEM images of HCMs and HCFMs. Both samples are spherical with a monodisperse size distribution. However, significant differences in particle size and surface morphology were observed, as shown in the inset images (high magnification) of Fig. 2. The 50 nm Fe_3O_4 nano-crystals remained on the surface of HCFMs after heat treatment, as shown in Fig. 2c (inset). HCMs had a smooth surface even after heat treatment, as shown in Fig. 2a (inset). The average diameter of HCFMs (4.40 μm) was larger than that of HCMs (3.99 μm). The shell thicknesses of HCMs and HCFMs are 202 nm and 268 nm, respectively. The average diameter and shell thickness of hollow particles increased while introducing Fe_3O_4 nano-crystals.

HRTEM images show the internal structure of HCFMs and Fe_3O_4 nano-crystals embedded in a carbon shell, as shown in Fig. 3. A slice of TEM sample with thickness of 100 nm made by focused ion beam was employed to observe the distributed Fe_3O_4 nano-crystals throughout the carbon shell. The diameter of the hollow space and the thickness of the carbon shell are 3.86 μm and 268 nm, respectively. Fe_3O_4 nano-crystals were distributed throughout the carbon shell, and their average diameter was 5 nm. The inset in Fig. 3 shows a high resolution HRTEM image of Fe_3O_4 nano-crystals distributed and embedded in amorphous carbon matrix. It also shows lattice fringe with a *d*-spacing of 0.25 nm, which corresponds to the (311) plane of cubic Fe_3O_4 crystal (JCPDS 75-1609).

Fig. 4 shows XRD patterns of the HCMs and HCFMs. The broad peak at $2\theta = 26°$ is a typical XRD pattern of amorphous carbon, as shown in Fig. 4a. For HCFMs, the main peaks are at $2\theta = 30.09°$, 35.42°, 43.00°, 54.05°, 57°, and 62.51°,which is consistent with the XRD pattern of a crystal Fe_3O_4, as shown in Fig. 4b. These results indicate that the HCFMs contain Fe_3O_4 nano-crystals, and that their crystalline phases are not transformed by heating at 600 °C for 7 h under nitrogen gas.

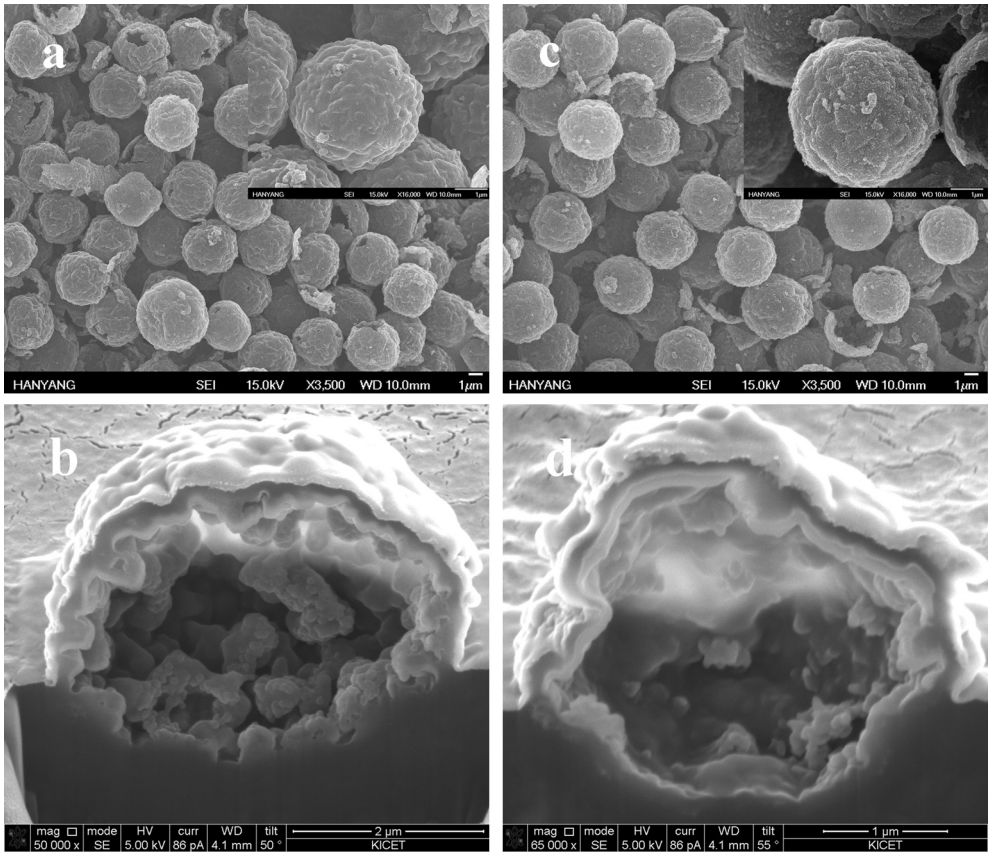

Fig. 2. SEM images of (a) HCMs, (c) HCFMs, and their cross-sectional images, (b) and (d).

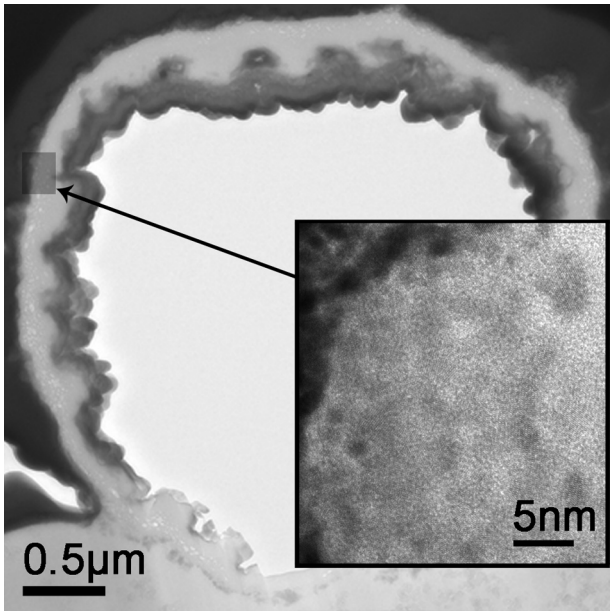

Fig. 3. HRTEM images of HCFM under low and high magnification (inset).

Fig. 5 shows TGA thermograms of the nano-sized Fe_3O_4 particles and HCFMs conducted under air atmosphere. A TGA thermogram corresponding to the nano-sized Fe_3O_4 particles showed slight weight loss of 0.7 wt. % from 50 to 700 °C. The as-prepared HCFMs sample showed two-step weight loss in the temperature region of 50–700 °C. The initial weight loss from HCFMs between 50 and 200 °C was probably due to the removal of surface hydroxyls and/or surface adsorbed water. The weight loss at higher temperature (300–500 °C)is mainly attributed to decomposition of amorphous carbon by reaction with O_2. The HCFMs loss amounted to about 90 wt. %, indicating that a mass of about 20 wt. % corresponds to the Fe_3O_4 portion of HCFMs.

3.2. Electrochemical properties

Fig. 6 shows CV curves of HCMs and HCFMs for the first three discharge/charge cycles in a voltage range of 3.0 to 0.0 V at a scan rate of 0.1 mV s^{-1}Fig. 6a shows that intercalation/deintercalation of Li^+ into the hard carbon phase mainly occurred in wide ranges of potential (0.0–1.0 V). The cyclic voltammogram of hard carbon did not show clear peaks, which corresponds to the insertion or extraction of Li ions [17,18]. In Fig. 6b, three reduction peaks are

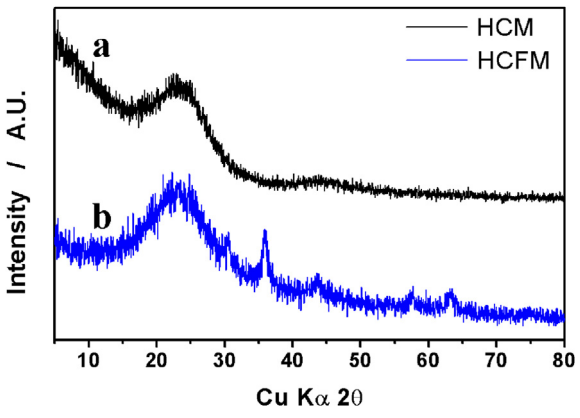

Fig. 4. X-ray diffraction patterns of (a) HCMs and (b) HCFMs.

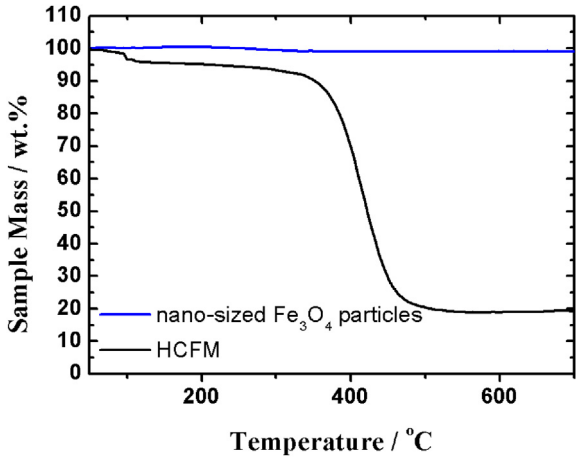

Fig. 5. TGA plots of HCFMs and nano-sized Fe_3O_4 particles under gaseous mixture of mainly air at heat in grate of 5 °C min^{-1}.

observed in the first cathodic scan for HCFMs. The two peaks around 1.5 V and 0.82 V are ascribed to the formation of $Li_xFe_3O_4$ [19,20]. The third strong peak at around 0.68 V may be associated with the reduction of Fe^{3+} and Fe^{2+} to Fe^0 and an irreversible reaction related to the decomposition of electrolyte [17]. During the first two cycles, irreversibility was due to the formation of amorphous Li_2O and the conversion of Fe_3O_4 to Fe [20].In the anodic process, two reversible peaks at about 1.6 V and 1.9 V correspond to the oxidation of Fe^0 to Fe^{2+} and Fe^{3+}, respectively. Fig. 6c and d displays voltage profiles of HCMs and HCFMs at a current rate of 0.05C for the first two cycles (SEI formation cycling), followed by three cycles at 0.1C. Overall, the voltage profiles of HCMs and HCFMs are similar to those of carbon materials and carbon/Fe_3O_4 composite materials. These results are well matched to the CV date, as shown in Fig. 6a and b. During the first five cycles, the specific capacities of HCFMs are higher than those of HCMs, indicating that introduced Fe_3O_4 nano-crystals may increase specific capacity. The reversible capacities of HCM and HCFM composite electrodes remained at around 457 and 660 mAh g^{-1},respectively, with fractional capacity fading in cycles three to five, as shown in Fig. 6c and d.

The rate performances of HCMs, HCFMs, and nano-sized Fe_3O_4 particles were evaluated by discharging at 0.2C and charging at various current rates in the voltage range between 0.02 and 3 V, as shown in Fig. 7. The composite electrode containing nano-sized Fe_3O_4 particles showed high discharge capacity of 1803 mAh g^{-1} at the initial cycle. However, it exhibited severe capacity fading with low coulombic efficiency in subsequent cycles due to large volume variation during the charge–discharge reactions. Conversely, HCMs and HCFMs showed good rate capabilities at all current rates (0.1–10C), as shown in Fig. 7.The high rate capabilities of HCM and HCFM electrodes are mainly attributed to their hollow structures, which have larger surface areas and shorter Li ion diffusion lengths during the lithiation and de-lithiation processes. In particular, the HCFM electrode exhibited a higher specific capacity of 501 mAh g^{-1} than the HCM electrode (304 mAh g^{-1}). It also demonstrated stable cycling even at a high current rate of 10C due to Fe_3O_4 nano-crystals homogeneously embedded in an amorphous carbon shell.

To confirm the cyclability of all electrodes at high current rate, the cycling performances of HCM, HCFM, and nano-sized Fe_3O_4 electrodes were tested and compared at a constant current rate of 10C for 100 cycles. As seen in Fig. 8, the discharge capacity of the pristine Fe_3O_4 electrode rapidly began decreasing at the second cycle, and remained at about 10 mAh g^{-1} until the 100th cycle.

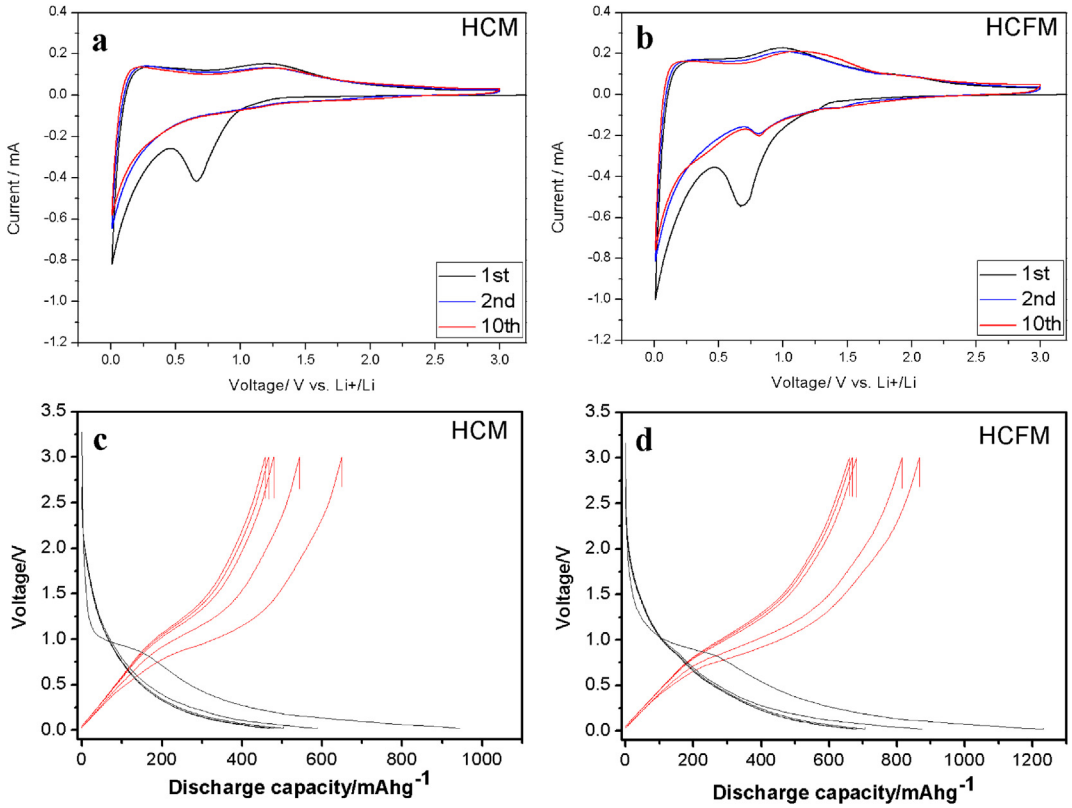

Fig. 6. Electrochemical performance of HCMs and HCFMs: cyclic voltammograms of (a) HCMs and (b) HCFMs with scan rate of 0.1 mV s^{-1}, and voltage profiles of (c) HCMs and (d) HCFMs at 0.1C with 0.02–3.0 V voltage.

Conversely, HCM and HCFM electrodes exhibited high specific capacities and excellent capacity retention at the same current rate of 10C with high coulombic efficiency of above 99%. The discharge capacity of HCFM electrodes was much higher at the 100th cycle than that of HCM electrodes. HCFM discharge capacities gradually increased from 328 mAh g^{-1} at the third cycle (after formation cycles) to 368 mAh g^{-1} at the 100th cycle, which is twice as high as the specific capacity (198 mAh g^{-1}) of HCM electrodes. The capacity increase during cycle is attributed to the reversible growth of a polymeric gel-like film on the active materials resulting from kinetically activated electrolyte degradation [4,21,22].The higher specific capacity and good reversible capacity retention of HCFMs are likely due to Fe_3O_4 nano-crystals embedded in the amorphous carbon shell, as mentioned above. The hollow structure of carbon microspheres provides a short diffusion length for Li ions while the carbon layer can accommodate volume changes due to Fe_3O_4 nanoparticles during the lithiation/de-lithiation process.

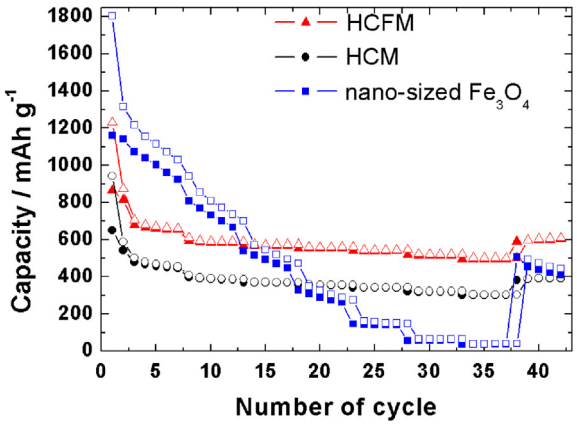

Fig. 7. Cycling performance of HCMs, HCFMs, and nano-sized Fe_3O_4 particles at various rate capabilities.

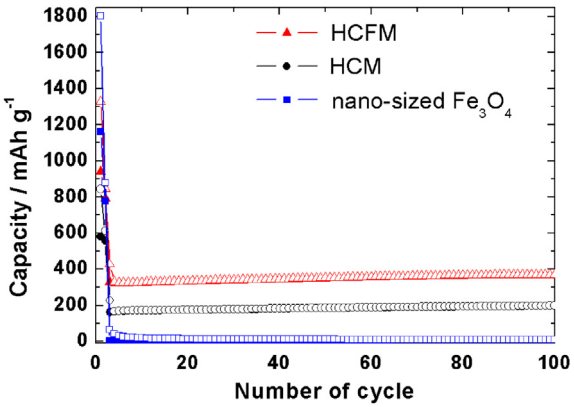

Fig. 8. Cyclic performance of HCMs, HCFMs, and nano-sized Fe_3O_4 particles at high current rate (10C).

4. Conclusions

In this study, monodispersed HCFMs were synthesized by heat treating as-prepared monodispersed HPMs with seeded polymerization. HCFMs were then used as anode materials for LIBs. The alkaline co-precipitation of iron salts was used to introduce Fe_3O_4 nano-crystals to the HPMs. After heat treatment, HCFMs that retained their intrinsic spherical shape and hollow structure were obtained. When compared to monodispersed HCMs in

electrochemical tests, both electrodes exhibited excellent cycling and rate performances. In particular, HFCMs retained a higher specific capacity than HCMs. Their capacity did not fade even after 100 cycles at a high current rate of 10C. These results are attributed to the hollow structure and introduced Fe_3O_4 nano-crystals. Therefore, we suggest utilization of HFCMs as a promising alternative anode material for high performance LIBs.

Acknowledgements

This work was supported by the National Research Foundation of Korea (NRF) grant funded by the Korea government (MEST) (No. 2012-0002074).

References

[1] B.B. Owens, W.H. Smyrl, J.J. Xu, J. Power Sources 81–82 (1999) 150–155.
[2] P. Poizot, S. Laruelle, S. Grugeon, L. Dupont, J.-M. Tarascon, Nature 407 (2000) 496–499.
[3] P. Poizot, S. Laruelle, S. Grugeon, L. Dupont, J.-M. Tarascon, J. Power Sources 97–98 (2001) 235–239.
[4] S. Laruelle, S. Grugeon, P. Poizot, M. Dolle, L. Dupont, J.M. Tarascon, J. Electrochem. Soc. 149 (2002) A627–A634.
[5] Y. He, L. Huang, J.S. Cai, X.M. Zheng, S.G. Sun, Electrochim. Acta 55 (2010) 1140–1144.
[6] G.H. Lee, J.G. Park, Y.M. Sung, K.Y. Chung, W.I. Cho, D.W. Kim, Nanotechnology 20 (2009) 295205–295209.
[7] T. Yoon, C. Chae, Y.-K. Sun, X. Zhao, H.H. Kung, J.K. Lee, J. Mater. Chem. (2011) 17325–17330.
[8] Q. Hao, D. Lei, X. Yin, M. Zhang, S. Liu, Q. Li, L. Chen, T. Wang, J. Solid State Electrochem. 15 (2011) 2563–2569.
[9] T. Muraliganth, A.V. Murugan, A. Manthiram, Chem. Commun. (2009) 7360–7362.
[10] H. Liu, G. Wang, J. Wang, D. Wexler, Electrochem. Commun. 10 (2008) 1879–1882.
[11] Q.Q. Xiong, Y. Lu, X.L. Wang, C.D. Gu, Y.Q. Qiao, J.P. Tu, J. Alloys Compd. 536 (2012) 219–225.
[12] S. Jin, H. Deng, D. Long, X. Liu, L. Zhan, X. Liang, W. Qiao, L. Ling, J. Power Sources 196 (2011) 3887–3893.
[13] J. Liu, D. Xue, Nanoscale Res. Lett. 5 (2010) 1525–1534.
[14] W. Zhang, X. Wang, H. Zhou, J. Chen, X. Zhang, J. Alloys Compd. 521 (2012) 39–44.
[15] Q. Zhang, Z. Shi, Y. Deng, J. Zheng, G. Liu, G. Chen, J. Power Sources 197 (2012) 305–309.
[16] J.W. Kim, K.D. Suh, Colloid Polym. Sci. 276 (1998) 870–878.
[17] B. Xu, L. Shi, X. Guo, L. Peng, Z. Wangc, S. Chen, G. Cao, F. Wub, Y. Yang, Electrochim. Acta 56 (2011) 6464–6468.
[18] V.G. Khomenko, V.Z. Barsukov, Electrochim. Acta 52 (2007) 2829–2840.
[19] L. Wang, Y. Yu, P.C. Chen, D.W. Zhang, C.H. Chen, J. Power Sources 183 (2008) 717–723.
[20] Y. Piao, H.S. Kim, Y.-E. Sung, T. Hyeon, Chem. Commun. 46 (2010) 118–120.
[21] G. Zhou, D.-W. Wang, F. Li, L. Zhang, N. Li, Z.-S. Wu, L. Wen, G.Q. (Max) Lu, H.-M. Cheng, Chem. Mater. 22 (2010) 5306–5313.
[22] P.L. Taberna, S. Mitra, P. Poizot, P. Simon, J.-M. Tarascon, Nat. Mater. 5 (2006) 567–573.